Fast Prediction of Aperture Efficiency and Sidelobe Levels in Shaped Reflector Systems through Model Based Output Space Mapping

Fast Prediction of Aperture Efficiency and Sidelobe Levels in Shaped Reflector Systems through Model Based Output Space Mapping

Dirk I. L. de Villiers[1], Marianna V. Ivashina[2], Rob Maaskant[2]
[1]Dept. Electrical and Electronic Engineering, Stellenbosch University, Stellenbosch, South Africa, ddv@sun.ac.za
[2]Dept. Systems and Signals, Chalmers University of Technology, Gothenburg, Sweden

***Abstract*—This paper presents a fast method to accurately predict the aperture efficiency and sidelobe levels of shaped dual reflector systems over a wide region of the shaping parameter space. Only a few full evaluations of the system, at different points in the shaping parameter space, are needed to construct the model used for the predictions. The output space mapping technique is used to correct the responses obtained from a simple geometric optics model of the system for any desired point in the shaping parameter space by using the expected aperture edge taper information available from the shaping mapping and the feed pattern. The method is evaluated for a range of feeds, frequencies, and parameter spaces and shown to provide significantly improved results over the geometric optics predictions, while being orders of magnitude faster than full wave or asymptotic methods.**

***Index Terms*—reflector antenna, aperture efficiency, radio astronomy, space mapping, reflector shaping.**

I. INTRODUCTION

The performance of large dual reflector ground station and radio telescope antennas may often be improved by shaping the dishes to provide a desired transformation of the primary feed pattern to the reflector aperture field distribution. For axially symmetric systems (of which offset systems with circular projected apertures may form a sub-set), the goal of shaping the dishes is normally to improve either the gain or the receiving sensitivity of the system while maintaining a specified sidelobe level (SLL) and polarization performance. The receiving sensitivity, or the ratio of effective aperture area and system noise temperature, is typically improved by shaping the reflector surfaces to produce a higher secondary pattern directivity and thus effective area [1], as well as by reducing the energy not intercepted by the reflector system and thus reducing the antenna noise temperature. It was shown recently that an offset Gregorian reflector system, configured to tip with the sub-reflector nearer the ground when pointing towards the horizon (feed-down configuration), shaped for optimal aperture efficiency will also have near optimal sensitivity [2]. Accurate and rapid calculations of both the aperture efficiency and SLLs are thus of great benefit in the design and optimization of such systems, among them the Square Kilometre Array (SKA) radio telescope currently under development [3], [4].

Space mapping has been used extensively in the design of microwave structures and other systems, with several variations on the basic idea currently in use [5], [6]. To the authors' knowledge space mapping has not been applied to the design of shaped reflector antenna systems before. The space mapping method uses a simple, or coarse, model to approximate an accurate, or fine, model of some physical phenomenon. The coarse model should be relatively accurate but very fast to evaluate, whereas the fine model should be very accurate but is typically slow to evaluate. Both models have the same input parameters. Discrepancies between the responses of the coarse and fine models are minimized by a so-called parameter extraction, which may take a variety of forms. These parameters are used to construct a surrogate model, which is the corrected coarse model at a certain position in the parameter space. An iteration of the space mapping process involves the optimization of the surrogate model to achieve a specified goal function, and the evaluation of the fine model at the optimum position. After each iteration the surrogate model is updated using the new fine model information, and the process is repeated until the surrogate and fine models have sufficiently similar responses at the optimum position in the parameter space.

In this work the responses of interest are the aperture efficiency and SLLs of a shaped offset Gregorian reflector system for a given primary feed pattern. A full physical optics (PO) and physical theory of diffraction (PTD) simulation with the commercial code GRASP [7] is used as the fine model, and the coarse model is constructed by mapping and integration of the primary feed radiation pattern as detailed in Sec. II-B. Parameters used to describe the dish shapes form the parameter space of interest over which an optimization is typically performed. A form of output space mapping (OSM) is used to correct the coarse model response, with the correction factor augmented by model based physical arguments to improve the accuracy over the entire parameter space by using only a few initial fine model evaluations. Specifically, information on the expected edge illumination of the main reflector dish is incorporated to model the severity of the expected diffraction effects. The method is evaluated for ideal Gaussian and simulated feed horn patterns, and shown to produce accurate surrogate models over large parameter spaces and frequency ranges.

II. Output Space Mapping Problem Description

A. Space Mapping Formulation

Following the notation and descriptions of OSM in [8] a surrogate model (of the aperture efficiency and SLLs in this case), $\boldsymbol{R}_{\mathrm{s}}(\boldsymbol{x})$, is constructed from the coarse model, $\boldsymbol{R}_{\mathrm{c}}(\boldsymbol{x})$, as

$$\boldsymbol{R}_{\mathrm{s}}^{(i)}(\boldsymbol{x}) = \boldsymbol{R}_{\mathrm{c}}^{(i)}(\boldsymbol{x}) + \boldsymbol{d}^{(i)} \tag{1}$$

with

$$\boldsymbol{d}^{(i)} = \boldsymbol{R}_{\mathrm{f}}(\boldsymbol{x}^{(i)}) - \boldsymbol{R}_{\mathrm{c}}^{(i)}(\boldsymbol{x}^{(i)}). \tag{2}$$

The correction term $\boldsymbol{d}^{(i)}$ ensures zero order consistency between the fine model response, $\boldsymbol{R}_{\mathrm{f}}$, and the surrogate model for the input parameters $\boldsymbol{x}^{(i)}$ (in this case parameters describing the mapping used for shaping the dishes) at the ith iteration of the algorithm, i.e., $\boldsymbol{R}_{\mathrm{f}}(\boldsymbol{x}^{(i)}) = \boldsymbol{R}_{\mathrm{s}}^{(i)}\left(\boldsymbol{x}^{(i)}\right)$. In many problems the correction term $\boldsymbol{d}^{(i)}$ is strongly dependent on the input parameters, and by using an input parameter invariant correction term the final surrogate model may become inaccurate away from the initial position where $\boldsymbol{d}^{(i)}$ was determined. To alleviate this issue an adaptive response correction procedure was proposed and demonstrated in [8], where (1) is formulated instead as $\boldsymbol{R}_{\mathrm{s}}^{(i)}(\boldsymbol{x}) = \boldsymbol{R}_{\mathrm{c}}^{(i)}(\boldsymbol{x}) + \boldsymbol{\Delta}_{\mathrm{r}}\left(\boldsymbol{x}, \boldsymbol{x}^{(i)}\right)$, and the input variable dependent correction term $\boldsymbol{\Delta}_{\mathrm{r}}\left(\boldsymbol{x}, \boldsymbol{x}^{(i)}\right)$ is calculated through an adaptive process to ensure a well matched surrogate and fine model at each iteration of the algorithm (and thus at each position in the parameter space of interest). In this work the idea is instead to formulate a correction term which is calculated directly from a physical model based transformation of the input variables as

$$\boldsymbol{R}_{\mathrm{s}}^{(i)}(\boldsymbol{x}) = \boldsymbol{R}_{\mathrm{c}}^{(i)}(\boldsymbol{x}) + \boldsymbol{\Delta}_{\mathrm{r}}\left(\alpha(\boldsymbol{x})\right). \tag{3}$$

The function $\alpha(\boldsymbol{x})$ in this case is a by-product of the coarse model calculation, with details given in Sec. II-C, and therefore requires very little additional computational effort.

B. Coarse Model Construction

The shaped dual reflector systems considered here are described by a mapping, P, from the feed field pattern, $G(\theta')$, to the aperture field distribution, $E(\rho)$ as $P : G \to E$. The mapping is axially symmetric, with the angle θ' measured from the feed axis and ρ the distance from the center of the projected, circular, main reflector aperture axis. The equation explicitly describing the mapping (in terms of power since the shaping algorithm enforces equal path lengths and thus a constant phase mapping) is given by [9]

$$|E(\rho, \phi)|^2 = \frac{|G(\theta', \phi)|^2 \sin\theta'}{V_{\mathrm{c}}\rho(\theta', \boldsymbol{x})\rho'(\theta', \boldsymbol{x})}, \tag{4}$$

with $\rho'(\theta', \boldsymbol{x})$ denoting the θ' derivative of ρ, and V_{c} a normalization constant. Equation (4) is given for a general feed radiation pattern, which may have azimuthal variations in ϕ. The input parameters in $\boldsymbol{x}$ are used to set up the function $\rho(\theta')$ - either explicitly or implicitly by specifying a desired aperture distribution for a given feed pattern. Once the aperture field has been calculated, the secondary pattern may be calculated by aperture integration.

Normally, feeds for reflector systems requiring axially symmetric secondary patterns have high BOR_1 efficiency [10], implying that the full antenna pattern can be described to a high degree of accuracy by the E- and H-plane cuts, or by Ludwig's third definition of co- and cross-polarization fields in the diagonal or inter-cardinal plane cut. Since the mapping to the aperture field is axially symmetric, the same is true for the aperture fields. In the diagonal plane, defined by $\phi = 45°$, the co- and cross-polar feed patterns, $\mathrm{CO}_{\mathrm{f}}(\theta')$ and $\mathrm{XP}_{\mathrm{f}}(\theta')$, are calculated as in [10, (9) and (10)], and are the mean and half the difference of the E- and H-plane patterns of the feed respectively. Using (4), the co- and cross-polar aperture field patterns, $\mathrm{CO}_{\mathrm{a}}(\rho)$ and $\mathrm{XP}_{\mathrm{a}}(\rho)$, are found by substituting $G(\theta', 45°)$ with $\mathrm{CO}_{\mathrm{f}}(\theta')$ and $\mathrm{XP}_{\mathrm{f}}(\theta')$ to find $\mathrm{CO}_{\mathrm{a}}(\rho)$ and $\mathrm{XP}_{\mathrm{a}}(\rho)$ as $E(\rho, 45°)$.

The aperture efficiency may be calculated as $\eta_{\mathrm{ap}} = \eta_{\mathrm{f}}\eta_{\mathrm{d}}$, with η_{f} denoting the feed efficiency (slight variation on the definition used in [10]), and η_{d} denoting the diffraction efficiency [11]. The feed efficiency is given by

$$\eta_{\mathrm{f}} = \frac{16\pi}{D^2 P_{\mathrm{r}}}\left|\int_0^{D/2} \mathrm{CO}_{\mathrm{a}}(\rho)\rho d\rho\right|^2, \tag{5}$$

with D the projected diameter of the main dish and P_{r} the total power in the feed pattern. An estimate of the diffraction efficiency, η_{d}, is obtained by using the generating unshaped dish system, used in in the specification of the shaped dish system [9], and the method explained in [11]. Note that, since the shaped system will produce slightly different curvatures and reflector edge positions than the generating unshaped system, the approximation for the diffraction efficiency may become less accurate for shaped systems. This issue is alleviated by the OSM described in the following section.

The SLLs are estimated from the secondary pattern obtained by aperture integration of the mapped feed pattern. It can be shown that the secondary pattern, given the aperture field distribution co- and cross-polar components in the diagonal plane, can be calculated for linear polarization as [12]

$$\begin{aligned}\mathbf{G}_{\mathrm{s}}(\theta, \phi) &= C\cos^2(\theta/2)[(E_x\cos\phi + E_y\sin\phi)]\hat{\mathbf{u}}_\theta \\ &+ C\cos^2(\theta/2)[(-E_x\sin\phi + E_y\cos\phi)]\hat{\mathbf{u}}_\phi,\end{aligned} \tag{6}$$

with C a normalization constant, θ and ϕ the spherical coordinate system variables in the axis of the secondary pattern, $\hat{\mathbf{u}}$ indicating directional unit vectors, and

$$\begin{aligned}E_x(\theta, \phi) &= E_{\mathrm{XP}}(\theta)\sin(2\phi) \\ E_y(\theta, \phi) &= E_{\mathrm{CO}}(\theta) - E_{\mathrm{XP}}(\theta)\cos(2\phi).\end{aligned} \tag{7}$$

The definition in (7) is for the y-polarized case, and may trivially be changed for the x-polarization. The secondary co- and cross-polarized patterns in the diagonal plane, E_{CO} and E_{XP}, are calculated from the corresponding aperture distributions as

$$\begin{aligned} E_{\mathrm{CO}}(\theta) &= 2\pi \int_0^{D/2} \mathrm{CO}_{\mathrm{a}}(\rho) J_0(k\rho\sin\theta)\rho d\rho \\ E_{\mathrm{XP}}(\theta) &= -2\pi \int_0^{D/2} \mathrm{XP}_{\mathrm{a}}(\rho) J_2(k\rho\sin\theta)\rho d\rho, \end{aligned} \tag{8}$$

where J_n indicates the Bessel function of the first kind of order n.

C. Model Based Output Space Mapping Correction

When analyzing the responses of shaped dual reflector systems, the main differences observed between the coarse and fine model efficiencies and SLLs, $\eta_{\mathrm{ap}}^{\mathrm{c}}$, $\eta_{\mathrm{ap}}^{\mathrm{f}}$, $\mathrm{SLL}^{\mathrm{c}}$, and $\mathrm{SLL}^{\mathrm{f}}$, are due to the effects of diffraction from the main and sub-reflector edges. These effects are only partially modeled in the coarse model (only sub-reflector diffraction is included in the efficiency model), and can therefore not be corrected by the standard input space mapping procedure. The SLLs are especially sensitive to small changes in pattern symmetry and aperture phase distributions, and these effects cannot be modeled adequately by the coarse models suggested here. Instead, OSM is performed to decrease the difference between the coarse and fine model responses. Since the main cause of the discrepancies between the models is assumed to be edge diffraction, which in turn is dependent on the strength of the edge illumination, this information can be incorporated when setting up the OSM correction term. In fact, the expected main reflector (and sub-reflector) illumination edge taper is already available from the mapping required during the coarse model calculation process.

The method suggested here involves the initial calculation of a few fine model response sets at $i_n = [1, 2, \cdots, N+1]$. N is the order of the approximation function to be used, with a description following later in this section. Ideally, the positions of the calculations should be chosen such that $\boldsymbol{x}^{(1)}$ corresponds to a position in the coarse model space where the mean main reflector edge taper, $\bar{t}$, is at a minimum and $\boldsymbol{x}^{(N+1)}$ where $\bar{t}$ is at a maximum. The rest of the points should be approximately equally spaced (in terms of $\bar{t}$) between these extremes. The edge taper is defined as

$$\bar{t} = \left\langle \frac{E(D/2, \phi)}{E(0, \phi)} \right\rangle, \tag{9}$$

with $\langle \cdot \rangle$ denoting the mean over ϕ, and $E(\rho, \phi)$ calculated from the feed pattern $G(\theta', \phi)$ using the mapping P. A correction term, $\boldsymbol{\Delta}_{\mathrm{r}}\left(\boldsymbol{x}^{(i_n)}\right)$, is calculated at each of the initial positions as

$$\boldsymbol{\Delta}_{\mathrm{r}}\left(\boldsymbol{x}^{(i_n)}\right) = \boldsymbol{R}_{\mathrm{f}}\left(\boldsymbol{x}^{(i_n)}\right) - \boldsymbol{R}_{\mathrm{c}}\left(\boldsymbol{x}^{(i_n)}\right) \tag{10}$$

to ensure zero order consistency between the fine model and the surrogate model responses at $\boldsymbol{x}^{(i_n)}$. Here the components of the response $\boldsymbol{R}$ correspond to the aperture efficiency and the SLL. For example, for the fine model,

$$\boldsymbol{R}_{\mathrm{f}}(\boldsymbol{x}) = \left[\eta_{\mathrm{ap}}^{\mathrm{f}}(\boldsymbol{x}) \quad \mathrm{SLL}^{\mathrm{f}}(\boldsymbol{x})\right]. \tag{11}$$

The correction terms will have the same form. Note that the frequency dependence is suppressed in this section since the method is repeated for each frequency of interest - all responses and input parameters may therefore be treated as scalars at each frequency point. Writing the correction term as a function of the taper as $\boldsymbol{\Delta}_{\mathrm{r}}(\bar{t})$, an Nth order polynomial fit is performed, using the support points $\bar{t}\left(\boldsymbol{x}^{(i_n)}\right)$ and $\boldsymbol{\Delta}_{\mathrm{r}}\left(\boldsymbol{x}^{(i_n)}\right)$, to find an approximated correction factor at any taper value $\boldsymbol{\Delta}_{\mathrm{r}}^{\mathrm{p}}\left(\bar{t}(\boldsymbol{x})\right)$. The implicit definition $\boldsymbol{\Delta}_{\mathrm{r}}(\bar{t})$ does not, in general, guarantee a single-valued function in $\bar{t}$ over the full space $\boldsymbol{x}$, whereas the polynomial approximation $\boldsymbol{\Delta}_{\mathrm{r}}^{\mathrm{p}}(\bar{t})$ is a single valued function over all $\bar{t}$. This may cause errors in the surrogate models when large parameter spaces are considered where differences between the coarse and fine models become invariant to $\bar{t}$. However, the surrogate model is typically significantly closer to the fine model over the large shaping parameter spaces, and the approximation improves in reduced parameters spaces. The accuracy of the suggested method will be evaluated for some practical example cases in the following section.

III. Examples

The shaped mapping used for the examples is described in [13, (2)], with the role of the input parameters in the mapping summarized here for clarity. The mapping, $P(\boldsymbol{x})$, is defined intrinsically in the sense that it maps a given feed pattern G to a specified aperture distribution E. The aperture distribution is controlled by the input parameters $\boldsymbol{x} = [b_\rho, \sigma_\rho]$, and it is a form of Gaussian distribution with an edge taper at radius $D/2$ controlled by b_ρ, but with a constant distribution in a central region bounded by the normalized radius σ_ρ. The feed pattern used here is a simple Gaussian pattern with a 12 dB edge taper. Any other feed pattern will, of course, be mapped to a different aperture distribution by the fixed mapping function.

All reflector systems analyzed in this work are based on one of the systems described in [4], with projected main reflector diameter, $D = 15$ m, maximum sub- and main reflector chord lengths 4 m and 18.2 m, projected spacing between the reflectors of 0.5 m, sub-reflector subtended angle of $\theta_{\mathrm{e}} = 58°$, and a sub-reflector extension of 20°. The extension is included because it will degrade the performance of the coarse models by yielding inaccurate diffraction efficiency results. The OSM applied here should correct for this effect.

A. Univariate Parameter Space

As an initial test, only the parameter controlling the aperture field edge taper is varied and an ideal feed pattern is used (i.e. the pattern for which the mapping was specified). The input parameter space investigated spans $b_\rho \in [1.38, 3.68]$, which corresponds to expected aperture edge tapers in $[-6, -16]$ dB. Fine, coarse, and surrogate models were calculated on the frequency range $f = [350 : 5 : 1050]$ MHz. To determine the order of the polynomial fit, N, the required correction factors, $\boldsymbol{\Delta}_{\mathrm{r}}(\bar{t})$, for efficiency and SLL were calculated over the full parameter space, and are shown in Fig. 1. From these results $N = 2$ was chosen (higher order polynomials do not typically improve the results), and the polynomial approximation correction factors, $\boldsymbol{\Delta}_{\mathrm{r}}^{\mathrm{p}}(\bar{t})$, are also shown (as well as the

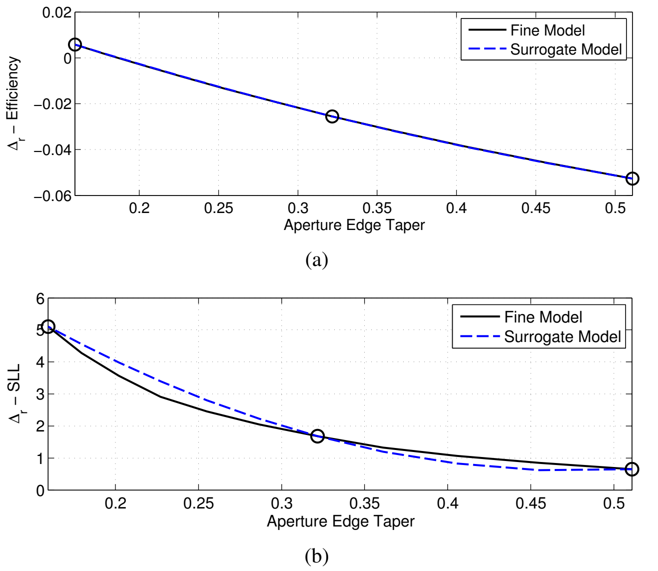

Fig. 1. Actual and polynomial fit correction factors, as a function of expected average aperture field edge taper (shown on a linear scale here to preserve the function shape), for the aperture efficiency in (a) and the SLL in (b). Support points for the interpolation are shown as circular markers.

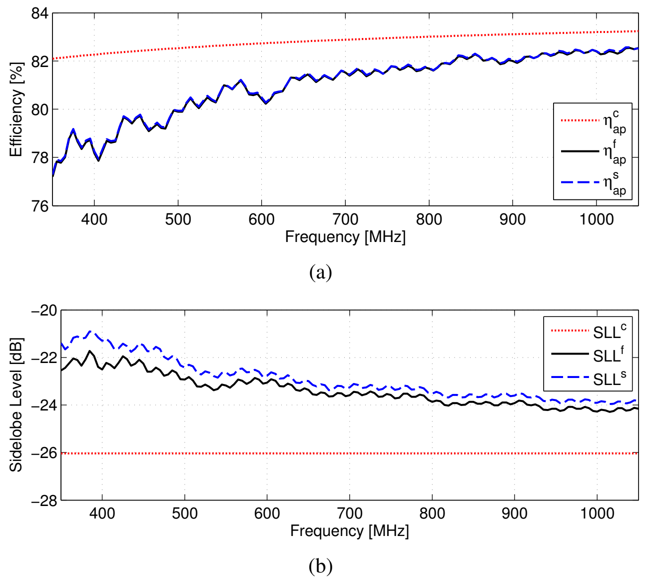

Fig. 2. Responses for the coarse, fine, and surrogate models of the aperture efficiency in (a) and the SLL in (b). Results are shown for the position in the parameter space with maximum surrogate model error.

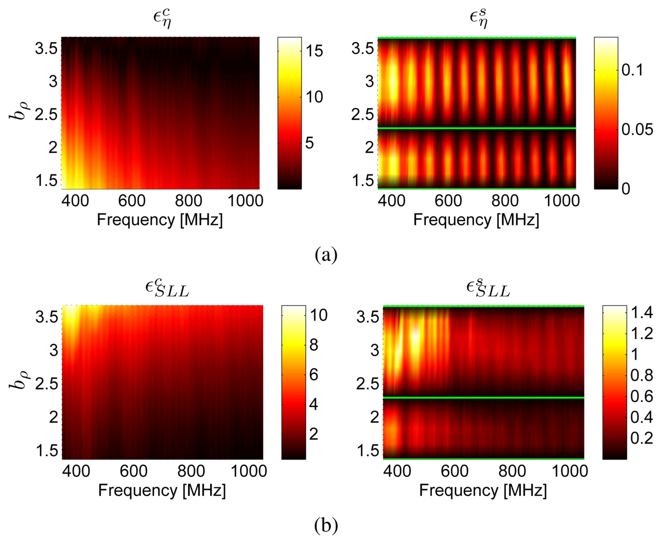

Fig. 3. Errors between the coarse and fine (on the left), and the surrogate and fine (on the right) models of the aperture efficiency in (a) and the SLL in (b). Support points for the surrogate model polynomial fit are shown as green lines. To preserve detail, the color scales are different for each of the plots.

positions of the support points). The coarse, fine, and surrogate responses of the efficiency and SLL are shown in Fig. 2 for the position in the parameter space where the largest difference between the fine and the surrogate model is observed. Note that the surrogate models model the fine frequency detail, caused mainly by interference between reflected energy from the main reflector and diffracted waves from the sub-reflector [14], which the coarse models completely ignore. Even in regions away from the support points in the parameter space the fine frequency detail is modeled well by the surrogate models. A plot of of the errors over the full parameter space and frequency range are shown in Fig. 3. For the efficiency the errors, ϵ_η, are normalized to the fine model response as $\epsilon^{\mathrm{c,s}}_\eta = |\eta_{\mathrm{c,s}} - \eta_{\mathrm{f}}|/\eta_{\mathrm{f}}$ for the coarse and surrogate models respectively. For the SLL the absolute errors are shown as $\epsilon^{c,s}_{\mathrm{SLL}} = |\mathrm{SLL}_{\mathrm{c,s}} - \mathrm{SLL}_{\mathrm{f}}|$. The bands of zero error, corresponding to the positions of the support points for the polynomial fit, are clearly visible for the surrogate models, and an increase in the error is observed for lower frequencies. This is due to the geometric optics approximation assumed for the coarse model failing for electrically small dishes. A significant improvement of the surrogate model over the coarse model for the entire parameter space and frequency range is observed.

B. Bivariate Parameter Space

As a more complete test the effect of varying the parameter σ_ρ was also investigated. Furthermore, in this section a simulated pattern of a quad-ridge flared horn (QRFH), such as the one described in [15], is used instead of an ideal Gaussian feed pattern. This feed was chosen specifically because it exhibits an elliptical pattern over most of the band, necessitating the use of the two aperture integration integrals in (8) instead of a simpler form required for an axially symmetric aperture distribution. The parameter space considered now extends that described in the previous subsection to include $\sigma_\rho \in [0, 0.6]$, and the frequencies investigated are limited to $f = [0.35, 0.75, 1.05]$ GHz. To conserve space the errors over the full parameter space are only plotted at 1.05 Ghz in Fig. 4, with the polynomial fit support points indicated by green markers. The expected region of insignificant error in the surrogate model is obvious through these points, and a marked improvement over the coarse model is observed over the full parameter space.

Smaller parameter spaces were also investigated to show

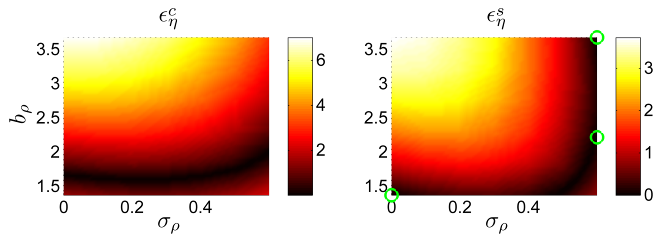

(a)

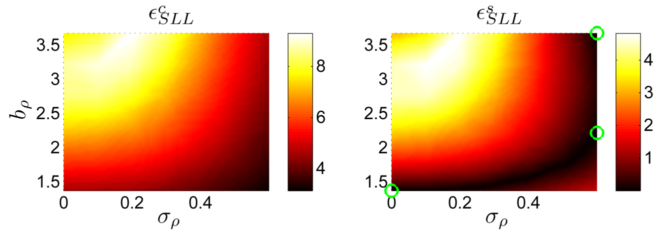

(b)

Fig. 4. Errors between the coarse and fine (on the left), and the surrogate and fine (on the right) models of the aperture efficiency in (a) and the SLL in (b). The frequency is 1050 MHz, and a QRFH is used as feed. The support points for the surrogate model polynomial fit are shown as green markers. Note the color scales are different for each of the plots to preserve detail.

the improved performance obtained in these cases. Typically, through the space mapping optimization process the parameter space of interest will decrease as the problem converges towards the optimum. To illustrate, the full parameter space in b_ρ and the minimum value of σ_ρ was kept, and the maximum value of σ_ρ was varied. The values of the maximum and average errors over the reduced parameter spaces are shown in Table. I. Again, the surrogate model improves the coarse model in all cases, with the increased errors observed at the highest frequency attributed to the low BOR_1 efficiency of the feed here (causing an inaccurate coarse model according to to comments in II-B). Important to note, though, is the marked improvement in surrogate model accuracy for reduced parameter spaces (as $\sigma_\rho \to 0.2$).

TABLE I
ERROR COMPARISON FOR COARSE AND SURROGATE MODELS FOR SEVERAL FREQUENCIES AND PARAMETER SPACE SIZES

Type	f (GHz)	Mean Error			Max Error		
		σ_ρ			σ_ρ		
		0.2	0.4	0.6	0.2	0.4	0.6
ϵ_η^c (%)	0.35	8.90	9.27	9.49	12.60	13.78	14.11
	0.75	6.17	6.09	5.71	11.00	11.00	11.00
	1.05	3.58	3.40	3.01	7.02	7.02	7.02
ϵ_η^s (%)	0.35	0.43	0.78	0.55	1.41	2.88	3.03
	0.75	0.08	0.43	1.57	0.33	0.86	2.77
	1.05	0.14	0.59	1.69	0.42	1.63	3.73
ϵ_{SLL}^c (dB)	0.35	2.93	2.67	2.37	5.57	5.57	5.57
	0.75	5.46	5.21	4.86	6.68	6.67	6.6
	1.05	7.33	6.90	6.21	9.31	9.31	9.31
ϵ_{SLL}^s (dB)	0.35	0.17	0.60	0.85	0.97	2.59	3.71
	0.75	0.13	0.63	1.03	0.64	1.51	2.63
	1.05	0.34	1.21	1.73	0.79	2.57	4.82

IV. CONCLUSION

This paper presented an OSM method where model based physical arguments are used to produce an accurate surrogate model, for aperture efficiency and SLL in shaped reflector systems, over the entire parameter space from only a few initial fine model evaluations. The surrogate model is constructed using fast geometric optics based predictions, augmented by an edge taper based correction, and is accurate over large parameter spaces describing the reflector shapes. Using this model, the full shaping parameter space may be quickly explored for optimization or parameter studies, without the need for slow fine model (typically PO) evaluations at each point in the parameter space.

ACKNOWLEDGMENT

This research was supported by a Marie Curie International Research Staff Exchange Scheme Fellowship within the 7th European Community Framework Programme under grant PIRSES-GA-2013-612599, Project MIDPREP.

REFERENCES

[1] A. G. Cha, “An offset dual shaped reflector with 84.5 percent efficiency,” *IEEE Trans. Antennas Propag.*, vol. AP-31, no. 6, pp. 896–902, Nov. 1983.

[2] D. I. L. De Villiers and R. Lehmensiek, “Offset Gregorian reflector shaping for optimum sensitivity,” in *Proc. Int. Conf. Electromagn. Adv. Appl. (ICEAA)*, Palm Beach, Aruba, Aug. 2014.

[3] P. E. Dewdney, P. J. Hall, R. T. Schilizzi, and T. J. L. W. Lazio, “The Square Kilometer Array,” *Proceedings of the IEEE*, vol. 97, no. 8, pp. 1482 – 1496, Aug. 2009.

[4] I. P. Theron, R. Lehmensiek, and D. I. L. de Villiers, “Towards an optics design for SKA,” in *IEEE AFRICON*, Mauritius, Sep. 2013.

[5] J. W. Bandler, Q. S. Cheng, S. A. Dakroury, A. S. Mohamed, M. H. Bakr, K. Madsen, and J. Sondergaard, “Space mapping: the state of the art,” *IEEE Trans. Microw. Theory Tech.*, vol. 52, no. 1, pp. 337–361, Jan. 2004.

[6] S. Koziel, Q. S. Cheng, and J. W. Bandler, “Space mapping,” *IEEE Microw. Mag.*, vol. 9, no. 6, pp. 105–122, Dec. 2008.

[7] TICRA, Copenhagen, Denmark. GRASP10, Version 10.0.1. [Online]. Available: http://www.ticra.com

[8] S. M. Koziel, J. W. Bandler, and K. Madsen, “Space mapping with adaptive response correction for microwave design optimization,” *IEEE Trans. Microw. Theory Tech.*, vol. 57, no. 2, pp. 478–486, Feb. 2009.

[9] P.-S. Kildal, “Synthesis of multireflector antennas by kinematic and dynamic ray tracing,” *IEEE Trans. Antennas Propag.*, vol. 38, no. 10, pp. 1587–1599, Oct. 1990.

[10] ——, “Factorization of the feed efficiency of paraboloids and cassegrain antennas,” *IEEE Trans. Antennas Propag.*, vol. AP-33, no. 8, pp. 903–908, Aug. 1985.

[11] D. I. L. de Villiers, “Offset dual-reflector antenna system efficiency predictions including subreflector diffraction,” *IEEE Antennas Wireless Propag. Lett.*, vol. 10, pp. 947–950, 2011.

[12] P.-S. Kildal, *Foundations of Antennas: A Unified Approach*. Studentlitteratur AB, 2000.

[13] D. I. L. De Villiers and R. Lehmensiek, “Sensitivity performance of several mappings in shaped offset Gregorian reflectors,” in *IEEE Int. Symp. Antennas and Propag. (APSURSI)*, Memphis, TN, Jul. 2014, accepted.

[14] D. I. L. de Villiers, “Prediction of aperture efficiency ripple in clear aperture offset Gregorian antennas,” *IEEE Trans. Antennas Propag.*, vol. 61, no. 5, pp. 2457–2465, May 2013.

[15] M. V. Ivashina, C. Bencivenni, O. Iopikov, and Y. J., “Optimization of the 0.35-1.05 GHz Quad-Ridged Flared Horn and Eleven feeds for the Square Kilometer Array baseline design,” in *Proc. Int. Conf. Electromagn. Adv. Appl. (ICEAA)*, Palm Beach, Aruba, Aug. 2014, pp. 513–516.